IEEE Access
Multidisciplinary | Rapid Review | Open Access Journal

Received February 4, 2019, accepted February 25, 2019, date of publication March 1, 2019, date of current version March 13, 2019.

Digital Object Identifier 10.1109/ACCESS.2019.2902240

Extraction of Rotor Eddy-Current Harmonic Losses in High-Speed Solid-Rotor Induction Machines by an Improved Virtual Permanent Magnet Harmonic Machine Model

CHONG DI, ILYA PETROV, AND JUHA J. PYRHÖNEN, (Senior Member, IEEE)
Department of Electrical Engineering, Lappeenranta University of Technology, 53851 Lappeenranta, Finland

Corresponding author: Chong Di (chong.di@lut.fi)

This work was supported in part by the Scholarship from the China Scholarship Council (CSC) under Grant CSC 201706690032.

ABSTRACT High-speed induction machines equipped with a solid steel rotor are capable of achieving a high-rotating speed than other types of machines, because of their simpler and more robust rotor structure. At the same time, however, the eddy-current losses in the solid rotor may be critical, because of the high conductivity of the rotor material, which makes it easy for axial eddy currents to travel in the solid rotor. To efficiently mitigate the rotor eddy-current losses, it is important to accurately determine the rotor eddy-current losses induced by a particular harmonic in advance. In this paper, an improved virtual permanent magnet harmonic machine (VPMHM) model equipped with a sinusoidally magnetized virtual magnet based on the finite element method (FEM) is proposed for determination of the rotor eddy-current harmonic losses. The 2-D fast Fourier transform was used to accurately analyze the time-spatial air-gap flux density harmonics. The VPMHM model was enhanced to ensure that it was able to exactly produce the required flux density harmonics in the air gap. Two algorithms for the improved VPMHM models with different hybrid excitations were proposed to determine the harmonic losses together with the other important harmonic behavior. The model was further investigated to separate the electromagnetic transients from different harmonics. Finally, the simulation time for the harmonic losses required by the enhanced VPMHM model was significantly reduced by separating the harmonic transients. All the results and conclusions presented in this paper are based on the FEM analysis.

INDEX TERMS Solid-rotor high-speed induction machine (IM), finite element method (FEM), 2-D fast Fourier transform, eddy-current losses, improved virtual permanent magnet harmonic machine (VPMHM).

I. INTRODUCTION

High-speed induction machines (IMs) equipped with a solid steel rotor have the advantage of running at a much higher rotational speed than other types of electrical machines, which are also frequently used in high-speed applications, such as permanent magnet synchronous machines (PMSMs) and switched reluctance machines (SRMs) [1]–[4]. It has been reported in [5] that the maximum rotor peripheral speeds that have been achieved in recent years for IMs (a solid rotor coated with a copper layer), PMSMs (rotor surface-mounted permanent magnets with a titanium sleeve), and SRMs (high-strength VCoFe laminations) are 367 m/s, 294 m/s, and 210 m/s, respectively. The solid steel rotor is more robust than other types of rotor structures, and thus, a high power density and torque density can be easily achieved, which makes the solid rotor IMs popular and widely used in many industrial applications, such as air compressors, submersible pumps, and turbos, as reported in [6]–[8].

When considering the mechanical construction, solid rotors are very attractive in high-speed IMs. Nevertheless, solid rotors degrade the electromagnetic performance of the machines because of the extra losses produced by the solid-rotor eddy currents. The high-conductivity rotor material contributes to the induced eddy currents (generated by the air-gap flux density harmonics) traveling in the axial direction

The associate editor coordinating the review of this manuscript and approving it for publication was Kan Liu.

2169-3536 © 2019 IEEE. Translations and content mining are permitted for academic research only.
Personal use is also permitted, but republication/redistribution requires IEEE permission.
See http://www.ieee.org/publications_standards/publications/rights/index.html for more information.

along the rotor shaft. Consequently, high eddy-current losses appear in the solid rotor because of the axial eddy currents. Typically, there are fewer measures available to efficiently cool the solid rotor than for cooling the stator. Therefore, more researchers have been focusing on reducing the solid-rotor eddy-current losses. Much of the present research concentrates on mitigating the rotor eddy-current losses by the design and use of different solid rotor structures, including the smooth solid rotor, slitted solid rotor, coated solid rotor, and caged solid rotor [5], of which the slitted solid rotor is the most popular one. It was stated in [9] that the slitted solid rotor could provide a higher efficiency with lower rotor eddy-current losses at a lower slip than the smooth solid rotor.

Moreover, there are some universal technologies that can be applied to mitigate the rotor eddy-current losses in high-speed IMs, such as rotor skews, semimagnetic wedges, and low-harmonic stator windings [10]–[12]. All these measures aim at minimizing the air-gap flux density harmonics. Correspondingly, to reduce the rotor eddy-current harmonic losses, it is essential to calculate and separate the harmonic losses from the total rotor eddy-current losses. Markovic and Perriard [13] proposed an analytical solution for the calculation of the rotor eddy-current losses in a slotless machine with current sheet excitation. However, because the solution was completely analytical, the iron saturation was neglected and the iron material was treated as linear. Markovic and Perriard [14] proposed an analytical method to determine the eddy-current losses in a configuration with a rotating permanent magnet. The configuration was a simple eddy-current brake based on the analytical method. However, only fundamental related loss was discussed in that paper. To predict the permanent magnet and sleeve eddy-current losses for a permanent magnet brushless machine, Zhu *et al*. [15] proposed an improved analytical method, which was capable of taking the magnetomotive force harmonics into account. However, the slotting effect was completely neglected in that research. All of these analytical methods have something in common; they are fast but not very precise because of different assumptions. Zhang *et al.* [16] and Koo *et al.* [17] utilized the 2-D FEM and 3-D FEM to accurately calculate the permanent magnet eddy-current losses, respectively. However, they were both not capable of extracting the harmonic losses from the total eddy-current losses, which is in highly demand in some real cases.

Recently, Di *et al.* [18] proposed a virtual permanent magnetic harmonic machine (VPMHM) model for solving the rotor eddy-current harmonic losses. The method is capable of generating a particular sinusoidal harmonic required in the air gap by simultaneously taking into account both the saturation and rotor damping effect (the effects of the rotor flux on the air-gap flux). The aim of the VPMHM is to generate a magnetic source, which is realized by setting a special virtual magnet in the FEM software. However, there were two main drawbacks when the VPMHM model was originally presented; one is related to the excitation on the virtual magnet and the other to the rotor permeability. To be more specific, a much lower flux density compared with the required flux density is generated in the air gap when a certain flux density harmonic is produced by the corresponding magnet excitation, as shown in [18, Fig. 2]. It means that the magnet excitation (remanence) has to be adjusted to achieve a correct flux density in the air gap because of the difference in the value of the remanence in the magnet and the actual flux density. Further, a constant rotor permeability with respect to the rotor saturation is used in the calculation of harmonic losses, which means that the rotor saturation is not fully accurately considered. These two problems can easily lead to some calculation errors as the rotor permeability is not evenly distributed on the rotor surface in the load condition.

To further mitigate the solid-rotor eddy-current losses more efficiently in the future, a method to extract the rotor harmonic losses is always in highly demand. When a particular rotor harmonic caused loss is known, effective measures can be taken to suppress the loss correctly. Because different harmonics are generated by different electromagnetic phenomena. The proposed improved VPMHM can provide an exact contribution of each harmonic to the overall rotor losses, that in turn helps to focus on the design aspects that cause the unwanted rotor losses. In this paper, an enhanced VPMHM (for solving the excitation problem) and a new computational algorithm (to solve the rotor permeability problem) are proposed to determine the rotor eddy-current harmonic losses more accurately in a 2-pole, 2 MW, 12000 r/min high-speed IM. The main advantage of the enhanced VPMHM is that it can accurately generate the required flux density and the rotor saturation can be considered in a proper manner, by avoiding possible errors caused by the wrongly assumed rotor damping effect and the saturation condition. First, the 2-D fast Fourier transform is employed to distinguish the air-gap flux density harmonic components. Two algorithms for the improved VPMHM models with different hybrid excitations are proposed to differentiate the harmonic losses together with other important harmonic behavior. Finally, it is shown that the improved VPMHM model is capable of distinguishing the harmonic transients from each other, which makes it possible to accelerate the simulation time with a negligible error.

II. AIR-GAP FLUX DENSITY HARMONIC ANALYSIS BY THE 2-D FAST FOURIER TRANSFORM ALGORITHM

A. INTRODUCTION OF THE HIGH-SPEED IM

In this paper, a 2-pole, 2 MW, 12000 r/min high-speed IM with a solid rotor is investigated. The machine was optimized and reported in detail in [18]. The total solid-rotor eddy-current losses are about 13.3 kW at the nominal load with a per-unit slip of about 0.005, both estimated by the 2-D FEM. For the sake of simplicity, the solid-rotor end effect is not taken into account in detail in this paper. Because the solid-rotor end effect should be accurately modeled by the 3-D FEM in principle. The 3-D FEM for a high-speed IM can

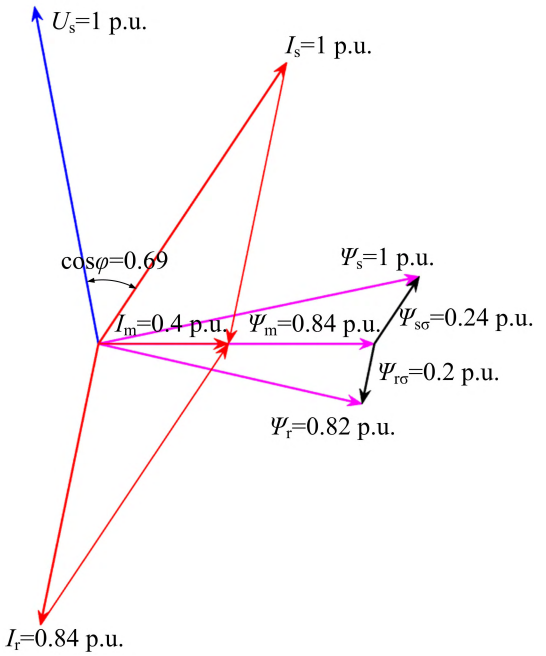

FIGURE 1. Vector diagram of the high-speed IM running at the nominal load with the stator phase voltage $U_s = 1$ p.u., the stator phase current $I_s = 1$ p.u., the rotor phase current $I_r = 0.84$ p.u., the magnetizing current $I_m = 0.4$ p.u., the stator flux linkage $\Psi_s = 1$ p.u., the rotor flux linkage $\Psi_r = 0.82$ p.u., the air-gap flux linkage $\Psi_m = 0.84$ p.u., the stator leakage flux linkage $\Psi_{s\sigma} = 0.24$ p.u., the rotor leakage flux linkage $\Psi_{r\sigma} = 0.2$ p.u., and the power factor $\cos\varphi = 0.69$. The stator resistance and the iron loss current are neglected.

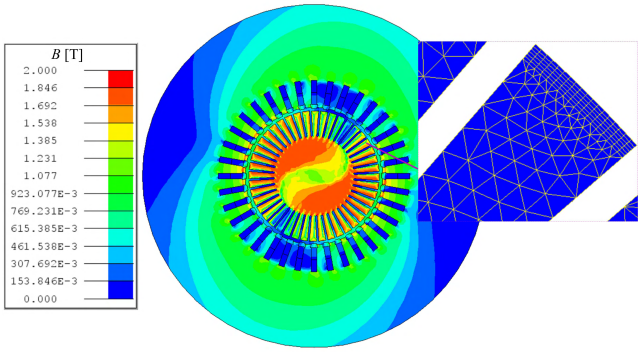

FIGURE 2. Flux density distribution of the high-speed IM at the nominal load in the steady state plotted by the 2-D FEM. It is referred to as "the normal FEM model" to distinguish it from the VPMHM model.

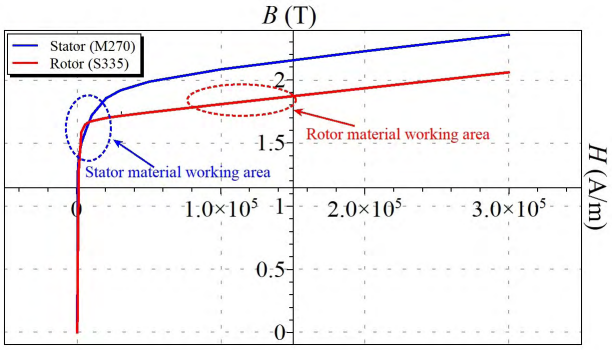

FIGURE 3. *B-H* curves of the stator and rotor materials.

be hardly achieved without an extremely powerful computer, because of the dense mesh and very small time step needed in transient solution. Fig. 1 shows the vector diagram of the machine at the nominal load. It can be seen that the machine has a power factor of 0.69 (it will be lower if the end effect is considered), whereas the leakage fluxes are relatively high. This clearly demonstrates the adverse effects of the methods used to reduce the rotor losses (especially the 7 mm air-gap length, the semimagnetic wedges, and the 4 mm wide rotor slot opening) on the machine performance.

Fig. 2 shows the flux density distribution of the high-speed IM at the nominal load. It can be seen that for accurate computation of the harmonic eddy-current losses, the rotor surface is densely meshed. There are six layers of dense mesh within the depth of 2 mm on the rotor surface. It can be also seen in the figure that the overall flux density in the rotor area is high. However, the overall flux density in the stator area is lower and some high-flux-density areas are only seen in the stator tooth tip areas. The stator material is M270-35A and the rotor material S355.

Fig. 3 shows the *B-H* curves of both the stator and rotor materials. It demonstrates that the stator and rotor are saturated at about 2.0 T and 1.7 T, respectively. Based on the flux density distribution at the nominal load in Fig. 2 and the *B-H* curves of the stator and rotor materials in Fig. 3, it can be concluded that the stator is still operating within the linear area of the material. The solid rotor, however, is highly saturated, which means that a significant proportion of the air-gap saturation harmonic is caused by the solid rotor itself instead of the stator.

B. AIR-GAP HARMONIC ANALYSIS AT THE NOMINAL LOAD

A suitable sampling frequency has to be applied to analyze the air-gap flux density harmonic content and to accurately calculate the rotor eddy-current losses. In this paper, the motor supply frequency is set to 200 Hz and the sampling frequency is 20000 Hz (the time step is 5×10^{-5} s), which means that the simulation can monitor the harmonics within the frequency from -10000 Hz to 10000 Hz based on the Shannon sampling theorem.

The eddy currents in the solid rotor are mainly generated by three different kinds of harmonics, viz. the stator winding harmonics, stator slot harmonics, and saturation harmonics. The source of the stator winding harmonics is the stator winding integer distribution, which for a 3-phase distributed winding can generate for instance the following harmonic orders: $+1$st, -5th, $+7$th, and -11th, where the positive sign means the same direction of rotation with the rotor and the negative sign denotes the opposite direction. The source of the stator slot harmonics, again, is the stator slot opening, which for a 36 stator slot machine can generate for instance the following

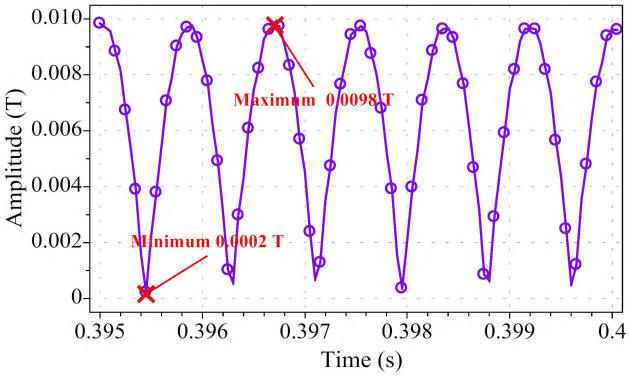

FIGURE 4. Amplitude of the 5th air-gap flux density harmonic at different time instants obtained by the traditional spatial fast Fourier transform at the nominal load.

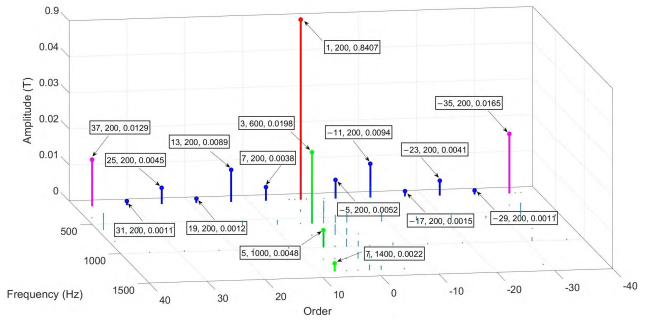

FIGURE 5. Air-gap flux density spectrum obtained by the 2-D fast Fourier transform at the nominal load.

harmonic orders: −35th, +37th, −71st, and +73rd. These two types of harmonics have the same frequency (200 Hz) as the supply frequency and a rotation velocity of Ω_{syn}/ν, where Ω_{syn} is the synchronous speed and ν is the harmonic order. The harmonics caused by saturation are the +3th, +5th, +7th, and so on, and the corresponding stator frequencies are 600 Hz, 1000 Hz, 1400 Hz, and so forth. Because the saturation harmonics are caused by the material properties of the stator and the rotor, they can be divided into stator saturation harmonics and rotor saturation harmonics. They both travel with the same speed of the synchronous speed. Therefore, it is very difficult to distinguish these two kinds of saturation harmonics from each other.

The analysis above reveals that there are some harmonics that have the same order but different frequencies; for example, the −5th winding harmonic operates with the 200 Hz supply frequency but the +5th saturation harmonic travels with the synchronous speed, creating a 1000 Hz phenomenon. This easily results in a calculation error with the traditional spatial fast Fourier transform. Fig. 4 shows the amplitude of the 5th air-gap flux density harmonic at different time instants by the traditional spatial fast Fourier transform at the nominal load. In this figure only the 5th harmonic is shown, since the error caused by the traditional Fourier transform is more obvious for the 5th harmonic than other harmonics. It is emphasized that all the harmonics discussed in this paper are normal components. It can be seen in the figure that at different time steps, different amplitudes of the 5th harmonic can be obtained when the spatial fast Fourier transform is applied. The harmonic can reach the minimum of 0.0002 T and the maximum of 0.0098 T, respectively. Such a variation may cause a mismatch to the actual harmonic component in the machine, which can lead to very different rotor eddy-current losses.

To define the air-gap flux density more accurately, the 2-D fast Fourier transform is applied in this paper. It has been widely used in the vibration analysis of electrical machines [19]. In fact, the air-gap flux density has both time-dependent and spatial properties, which means that they are determined both by frequency and order. For example, the −5th stator harmonic (200 Hz) travels slowly in the air gap in the negative direction, whereas the +5th saturation harmonic (1000 Hz) travels fast in the positive direction. The 2-D fast Fourier transform can provide a fast Fourier transform both in the time and spatial domains at the same time, which makes it possible to correctly determine the harmonics. Fig. 5 illustrates the air-gap flux density spectrum plotted by the 2-D fast Fourier transform at the nominal load. The red, blue, pink, and green bars in Fig. 5 denote the fundamental (which also belongs to the stator winding harmonics and it is emphasized here because of the fundamental property), the stator winding harmonics, the stator slot harmonics, and the saturation harmonics, respectively. It is emphasized that it is still not possible to distinguish the stator and rotor saturation harmonics from Fig. 5 because they are of the same frequencies and orders. However, as shown in Fig. 3, the stator is not saturated yet but the rotor is saturated, which indicates that most of the saturation harmonics belong to the rotor saturation harmonics. The rotor saturation harmonics do not cause any rotor eddy-current losses. The saturation harmonics will be further explained and discussed in Section III-B.

In addition, with the sampling frequency of 20000 Hz, the upper limit of the rotor-eddy current frequency is 10000 Hz. As shown in Fig. 5, the first-order stator slot harmonics (the −35th and +37th harmonics) are considered; they can both cause a 7200 Hz rotor eddy current. It is not possible to calculate the higher order harmonic eddy-current losses with the current sampling frequency. For example, the second-order stator harmonics, the −71st and +73rd ones, can generate a 14400 Hz rotor eddy current. This indicates that all the solid-rotor eddy-current losses can be considered to be caused by the harmonics shown in Fig. 5, especially the stator winding harmonics (containing the fundamental) and the stator slot harmonics.

III. IMPROVED VPMHM MODEL WITH HYBRID EXCITATION

A. IMPROVED VPMHM MODEL

Fig. 6 shows the improved VPMHM model for the separation of the rotor eddy-current harmonic losses. It is mainly aimed at solving the excitation problem, that is, the nonconformity

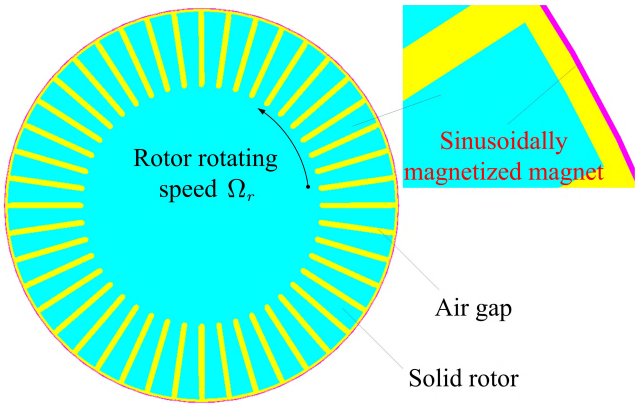

FIGURE 6. Improved VPMHM model for determination of the rotor eddy-current harmonic losses.

between the excitation (remanence) of the magnet and the actual air-gap flux density. It can been seen in Fig. 6 that the improved VPMHM model mainly contains three parts; the whole solid rotor, the air gap, and the sinusoidally magnetized magnet. The rotor has a rotating speed of Ω_r. However, the magnet is fixed, which is different from the rotating magnet presented in [18]. The rotating magnet is used to simulate the rotating property of the air-gap harmonic magnetic fields. Instead of applying a rotating magnet, the rotating property of the harmonics is directly taken into account by the excitation on the magnet with a time-varying signal. The excitation on the magnet can be expressed as

$$b_\nu(\theta, t) = \hat{B}_\nu \cos\left(\nu\theta - \frac{2\pi f_\nu t}{\nu} - \varphi_\nu\right) \tag{1}$$

where θ is the stator position, t is time, and ν is the order of the air-gap flux harmonic. $\hat{B}_\nu, f_\nu$ and φ_ν are the amplitude, stator current frequency, and initial phase angle of the νth harmonic, respectively.

A very thin virtual magnet as shown in Fig. 6 is employed to generate the same value of flux density in the air gap as that of the excitation (remanence) on the magnet. The thickness of the magnet is about 2 mm and the relative permeability of the material is 10^{-30}. The magnet is very thin owing to the algorithm of the software (Altair Flux) used in this paper. When the magnet is magnetized with a constant flux density, the software can only guarantee that the middle of the magnet (the middle of the pink ring in Fig. 6) has a constant value. Therefore, only when the thickness of the magnet is small enough, the flux density traveling from the inner surface of the magnet to the air gap will get close to the excitation on the magnet. The very low relative permeability can ensure a strong enough magnetic voltage in the circuit, which guarantees a robust flux density in the air gap to make the flux density in the magnet almost the same as its remanence.

Table 1 lists the air-gap flux density generated by the improved VPMHM model. The target amplitude denotes the required air-gap flux density, which is obtained by the 2-D fast Fourier transform, as shown in Fig. 5. It is also the excitation (remanence) for the sinusoidally magnetized magnet as shown in Fig. 6. The obtained amplitude in Table 1 denotes the air-gap flux density generated by the improved VPMHM model with the excitation (target amplitude). The table shows that the obtained amplitude is almost the same as the target amplitude, which can ensure an accurate computation of the solid-rotor eddy current losses.

TABLE 1. Air-gap flux density generated by the improved VPMHM model.

Order	Target amplitude, T	Obtained amplitude, T	Error, %
+1	0.8407	0.8425	+0.21
−5	0.0052	0.0052	–
+7	0.0038	0.0038	–
−11	0.0094	0.0094	–
+13	0.0089	0.0089	–
−17	0.0015	0.0015	–
+19	0.0012	0.0012	–
−23	0.0041	0.0041	–
+25	0.0045	0.0045	–
−29	0.0011	0.0011	–
+31	0.0011	0.0011	–
−35	0.0165	0.0164	−0.61
+37	0.0129	0.0128	−0.78

B. HYBRID EXCITED VPMHM MODELS FOR DETERMINATION OF ROTOR EDDY-CURRENT HARMONIC LOSSES

The improved VPMHM can generate a very precise air-gap flux density. To accurately determine the rotor eddy-current harmonic losses, an appropriate rotor relative permeability has to be considered at the nominal load. Because the penetration depth for a rotor eddy-current harmonic is directly affected by the rotor relative permeability, the penetration depth for a particular νth harmonic listed in Table 1 can be expressed as [20] and [21]

$$\delta_\nu = \frac{1}{\sqrt{\pi\mu_0\mu_r\sigma f\,|1-\nu\,(1-s)|}} \tag{2}$$

where μ_0 is the vacuum permeability, μ_r is the relative permeability of the rotor material, σ is the rotor solid-steel conductivity, f is the supply frequency, and s is the per-unit slip. $f\,|1-\nu\,(1-s)|$ is the rotor eddy-current harmonic frequency caused by the νth air-gap flux density harmonic.

Fig. 7 shows the distribution of the rotor incremental relative permeability at every node at the nominal load estimated by the 2-D FEM. The rotor incremental relative permeability ($dB/\mu_0 dH$) is described instead of the apparent relative permeability ($B/\mu_0 H$), because it is capable of describing the material property within a small domain, compared with the latter. Because the latter describes the relative permeability with the differences measured from the origin. The incremental relative permeability can more accurately reflect the saturation condition on a certain point of the rotor material. It is clearly shown in Fig. 7 that the incremental relative permeability is not evenly distributed on the solid rotor, which means, according to (2), that the penetration depths for a particular harmonic are different in different rotor positions.

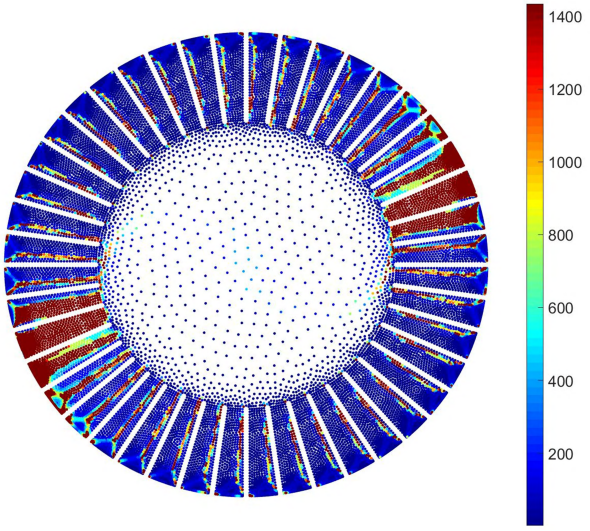

FIGURE 7. Distribution of the rotor incremental relative permeability at every node at the nominal load.

Therefore, accurate modeling of the rotor permeability is of critical importance.

A special computational algorithm based on hybrid excited VPMHM models is proposed to solve the rotor permeability problem. Fig. 8 shows the main procedure of the determination of solid-rotor eddy-current harmonic losses by the improved VPMHM models with hybrid excitation. There are two kinds of hybrid excited models. One is termed ''the increased harmonic hybrid excited model'' and the other ''the reduced harmonic hybrid excited model''. The details of the two models are shown in Fig. 8. Common to the two models is that all the hybrid excitations for the models contain the fundamental of the air-gap flux density. The fundamental in the hybrid exictiation is especially used to model the rotor saturation or the non-linear behavior of the material. As the amplitude of the fundamental of the air-gap flux is the largest, the rotor will automatically generate the corresponding rotor main magnetic field, when the fundamental is configured in the air gap by the VPMHM models. This means that the rotor main damping effect is considered automatically and the rotor itself sets the corresponding operating point (the corresponding area in the rotor material *B-H* curve) in the rotor material. Further, when the rotor is operating with the corresponding air-gap flux density harmonics, certain points within the rotor area automatically fit the *B-H* curve. This shows, again, that the rotor saturation has already been considered. Therefore, the permeability distribution in the rotor area and the rotor saturation are both taken into account accurately by the fundamental component excitation. Hence, the harmonic losses can be calculated by the loss difference between Model 1 and Model 2, as shown in Fig. 8. Nevertheless, the stator saturation is completely ignored because the stator does not contribute much to the saturation at the nominal load and it is difficult to get the exact stator saturation harmonic.

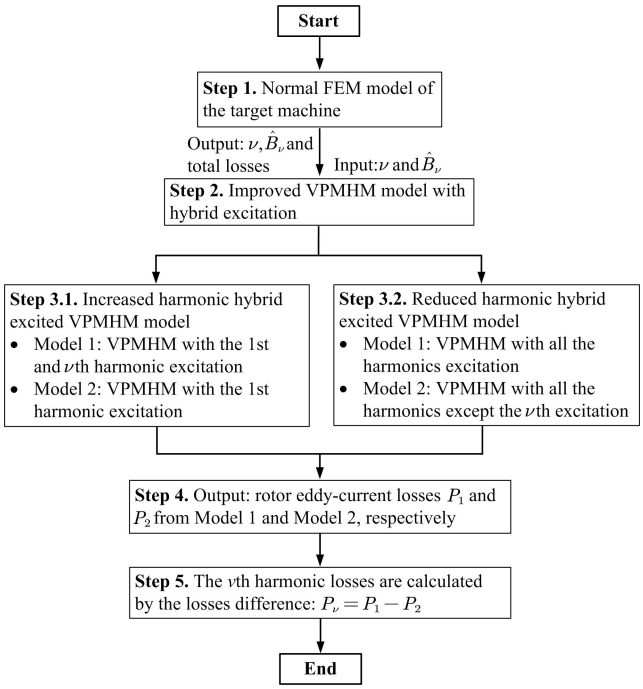

FIGURE 8. Procedure of the determination of solid-rotor eddy-current harmonic losses by the improved VPMHM models with hybrid excitation.

The difference between the increased and reduced harmonic hybrid excited VPMHM models is that the former only considers the fundamental effect on the rotor permeability and the latter all the harmonic effects as listed in Table 1 when computing the solid-rotor eddy-current harmonic losses. Because the fundamental effect on the rotor permeability is dominating, the losses calculated by the increased and reduced harmonic hybrid excited VPMHM models should be close to each other. Hence, the losses provided by the two models should verify each other.

IV. DETERMINATION OF ROTOR EDDY-CURRENT HARMONIC LOSSES BY DIFFERENT VPMHM MODELS

A. ROTOR EDDY-CURRENT HARMONIC LOSSES OBTAINED BY THE INCREASED HARMONIC HYBRID EXCITED VPMHM MODEL

By applying the improved VPHMH model with hybrid excitation, the rotor eddy-current harmonic losses can be determined accurately. Fig. 9 shows the harmonic eddy-current losses obtained by the increased harmonic hybrid excited VPMHM model at the nominal load. The fundamental loss (10842 W) is the highest one because the fundamental is very large and the corresponding loss belongs to the slip loss. The -5th and $+7$th harmonic losses are 344 W and 132 W, respectively. They are well suppressed by the short pitch winding ($y_Q = 5/6$). The -11th and $+13$th harmonic losses are 566 W and 430 W, respectively. They are the highest harmonic losses except for the fundamental loss. Further, although the first stator slot harmonics (the -35th and $+37$th harmonics) are significantly mitigated by the semimagnetic

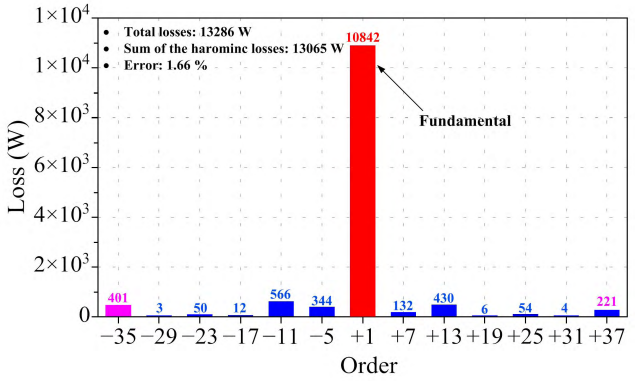

FIGURE 9. Rotor eddy-current harmonic losses obtained by the increased harmonic hybrid excited VPMHM model at the nominal load.

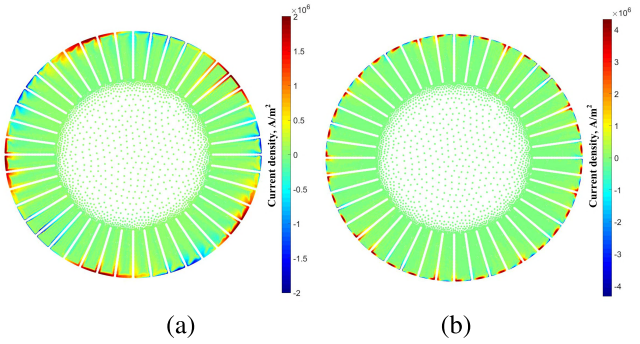

FIGURE 10. (a) Rotor eddy-current density distribution caused by the −5th harmonic at the nominal load estimated by the improved VPMHM model. (b) Rotor eddy-current density distribution caused by the +35th harmonic at the nominal load estimated by the improved VPMHM model.

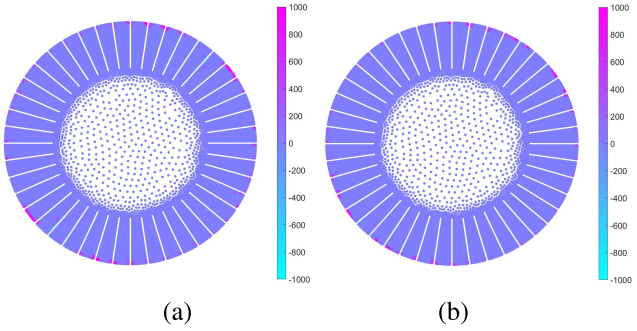

FIGURE 11. (a) Rotor incremental relative permeability distribution caused by the −5th harmonic at the nominal load estimated by the improved VPMHM model. (b) Rotor incremental relative permeability distribution caused by the +35th harmonic at the nominal load estimated by the improved VPMHM model.

wedges, they still cause high eddy-current losses (401 W and 221 W, respectively) in the solid rotor. Because the rest of the harmonics do not cause considerable losses, they are not discussed in detail. The total solid-rotor eddy-current losses are 13286 W calculated by the normal FEM model, as defined and shown in Fig. 2 and Fig. 8. The sum of all the harmonic losses computed by the increased harmonic hybrid excited VPMHM model is 13065 W, which means that the proposed method is accurate enough from the viewpoint of the FEM; the difference between these two models is only 221 W and the error is about 1.66%. This 221 W loss may be generated by the other harmonics including the stator saturation harmonic.

With the improved VPMHM model it is possible to obtain the rotor eddy-current distribution caused by a particular harmonic. Fig. 10 shows the rotor eddy-current density distributions caused by the −5th and +35th harmonics at the nominal load. The rotor eddy-current density distribution is also determined by the algorithm shown in Fig. 8. To be more specific, it is the distribution of the eddy-current density difference between the outputs of Model 1 and Model 2 in Fig. 8. It is clearly shown in Fig. 10 that the eddy current caused by the −5th harmonic penetrates deeper than that of the +35th harmonic, which matches (2) quite well, as the −5th harmonic causes a much lower rotor eddy-current frequency. Fig. 10 also reveals that the rotor eddy-current penetration depth is different in different rotor positions. The rotor eddy current penetrates deeper when the rotor relative permeability is lower. However, the amplitude of the eddy current generated by the +35th harmonic is larger than that of the −5th harmonic, which can be explained by the high eddy-current frequency. Finally, the −5th and +35th harmonics generate 344 W and 401 W rotor eddy-current harmonic losses, respectively.

Following the same logic for obtaining Fig. 10, the distributions of the rotor incremental relative permeability caused by the harmonics can be acquired as shown in Fig. 11. The figure shows that both the −5th and +35th harmonics can hardly change the rotor incremental relative permeability; it only increases in very small regions on the rotor surface within the corresponding penetration depth. The results show that the rotor is highly saturated and the saturation together with the correct relative permeability has already been considered by the fundamental of the hybrid excitation. Further, it indicates that the rotor eddy-current losses computed by the increased and reduced harmonic hybrid excited VPMHM models should have similar results, because the rotor incremental relative permeability cannot be affected much by the high-order harmonics.

B. ROTOR EDDY-CURRENT HARMONIC LOSSES OBTAINED BY THE REDUCED HARMONIC HYBRID EXCITED VPMHM MODEL

The rotor eddy-current harmonic losses determined by the reduced harmonic hybrid excited VPMHM model can be obtained with the algorithm shown in Fig. 8. The computational procedure is similar to that of the increased harmonic hybrid excited VPMHM model. Therefore, it is not discussed in detail here. Table 2 compares the rotor eddy-current harmonic losses determined by these two models, where Loss (inc.) and Loss (red.) denote the losses calculated by the increased harmonic VPMHM model and the reduced

TABLE 2. Comparisons of rotor eddy-current harmonic losses by different VPMHM models.

Order	Rotor induced frequency, Hz	Loss (inc.), W	Loss (red.), W	Error, %
+1	0	10842	10842	–
−5	1200	344	322	−6.4
+7	1200	132	134	+1.5
−11	2400	566	560	−1.1
+13	2400	430	426	−0.9
−17	3600	12	14	–
+19	3600	6	8	–
−23	4800	50	55	–
+25	4800	54	55	–
−29	6000	3	3	–
+31	6000	4	5	–
−35	7200	401	417	+4.0
+37	7200	221	238	+7.7
Total	–	13065	13079	+0.1

harmonic VPMHM model, respectively. Some errors are not listed in the table, either because the error is zero or the losses themselves are very small and can thus be neglected. There is a tendency that the increased harmonic VPMHM model gives more losses for the low-order harmonics. The reduced harmonic VPMHM shows more losses for the high-order harmonics. However, these two methods yield almost the same losses for both the total losses and a particular harmonic loss with very small errors. Moreover, the total losses computed by these VPMHM models (13065 W and 13079 W) are consistent with those (13286 W) obtained from the normal FEM model. Both the results can be considered to validate the accuracy of these two models.

C. DISCUSSION ON THE ACCELERATION OF THE SIMULATION TIME

The improved VPMHM with hybrid excitation proves to be accurate enough for the determination of solid-rotor eddy-current harmonic losses. It is also capable of obtaining the penetration depth on the rotor surface for a particular harmonic. However, the model also has some drawbacks; especially the simulation speed is low. Because of the good mesh quality and a very small time step, the normal FEM model as shown in Fig. 8 takes about 20 h (8000 steps) by a workstation equipped with Intel(R) Xeon(R) W-2135 CPU @ 3.70 GHz and 256 GB RAM before the machine fully reaches its steady state. ''Steady state'' here means that all the electromagnetic characteristics (e.g. torque, rotor speed, and stator current) reach the steady state. One particular improved VPMHM model almost takes the same amount of time as the normal FEM model because of the long transient caused by the fundamental during the simulation. Finally, it takes about 280 h in total including one normal FEM model and thirteen improved VPMHM models. It is not acceptable for some cases, especially certain industrial applications. Therefore, a critical problem is how to accelerate the simulation.

An option is to use the frozen permeability method to accelerate the simulation time. The method applies the rotor permeability distribution from the steady state at the beginning of the simulation so that the the steady state can be reached very quickly. The frozen permeability method has been widely used in PMSMs for instance for reluctance torque analysis and d-q inductance calculation as reported in [22] and [23]. However, this kind of a method is not suitable for the IM, especially the solid-rotor IM. This is explained by the fact that in the solid-rotor IM there are three main types of transient; eddy-current transient, magnetic field transient, and electric field transient. These three transients have to match and follow each other during the simulation, or otherwise, the convergence of the simulation could be lost. The improved VPMHM models with frozen permeability were also simulated in this study, and it was found that the results for the models were divergent.

Another method is based on the possibility of the improved VPMHM model to distinguish the harmonic behaviors (e.g. losses, penetration depth, and permeability) from an actual machine. It is even possible to distinguish the harmonic transients by the improved VPMHM model. Taking the increased harmonic hybrid excited VPMHM model as an example, Fig. 12 shows the rotor eddy-current density distribution caused by the fundamental and −5th harmonic at different time instants during transients from 0.05 s to 0.40 s. Fig. 12(a) reveals that when the time increases, the fundamental eddy current penetrates gradually deeper before it fully reaches the steady state. The eddy current has already penetrated into the rotor yoke area at 0.05 s. For the rest of the simulation time from 0.05 s to 0.40 s, the eddy current on the rotor surface remains almost the same, which means that most of the simulation time is used for the transient of the eddy current in the rotor yoke area caused by the fundamental from 0.25 s to 0.40 s. This is due to the fact that the fundamental has a much higher amplitude and penetrates much deeper at a very low slip. Consequently, the rotor suffers from a strong damping effect, and a much longer time period is needed for the fundamental transient. Fig. 12(b) shows that the rotor eddy current generated by the −5th harmonic remains almost the same after 0.05 s, because the penetration depth is relatively small and it is reached quite fast. The phenomenon indicates that the transients for the fundamental and high-order harmonics are different and the high-order harmonics have much shorter transients. In that case, it is possible to obtain the harmonic losses only during the transient before it fully reaches the steady state.

Fig. 13(a) shows the main high-order harmonic rotor eddy-current losses during the transient. The fundamental is not shown because it fully reaches the steady state only after about 0.40 s. The rest of the harmonic losses are not shown in the figure either because the losses are not high enough. It can be seen that the harmonic losses at 0.05 s are close to those in the steady state. After 0.25 s, all the harmonic losses remain almost the same, which means that all the harmonics complete their transients at around 0.25 s. Fig. 13(b) shows the total rotor eddy-current losses including the fundamental and all the harmonics listed in Table 1 during the transients. The fundamental loss is constant (10842 W) obtained

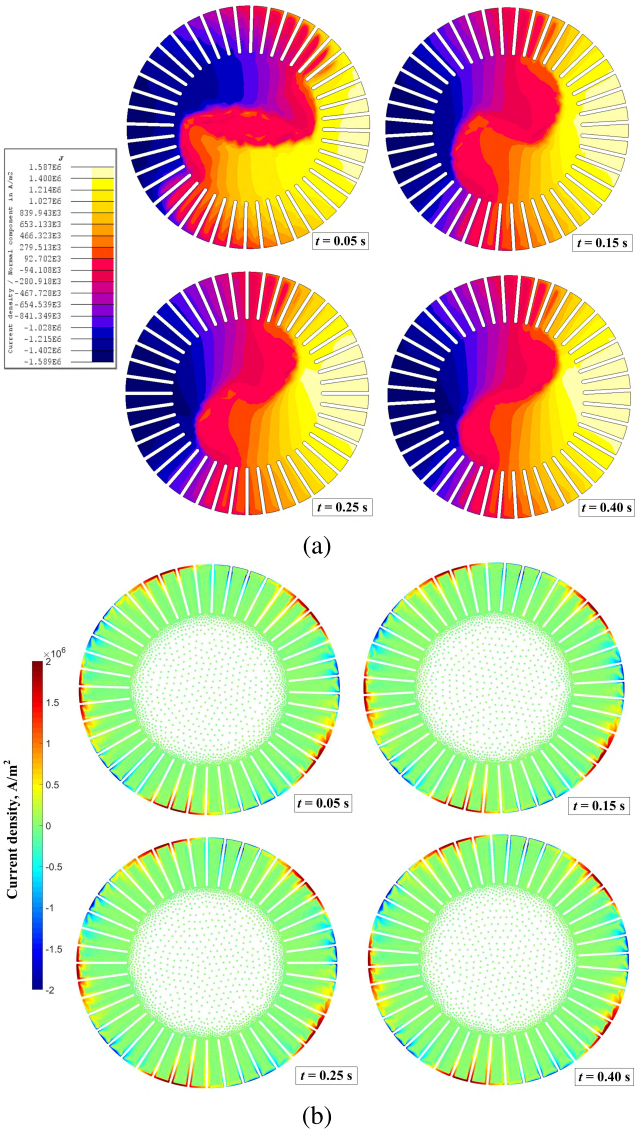

FIGURE 12. (a) Rotor eddy-current density distributions caused by the fundamental during the transient from 0.05 s to 0.40 s estimated by the increased harmonic hybrid excited VPMHM model. (b) Rotor eddy-current density distributions caused by the −5th harmonic during the transient from 0.05 s to 0.40 s estimated by the increased harmonic hybrid excited VPMHM model.

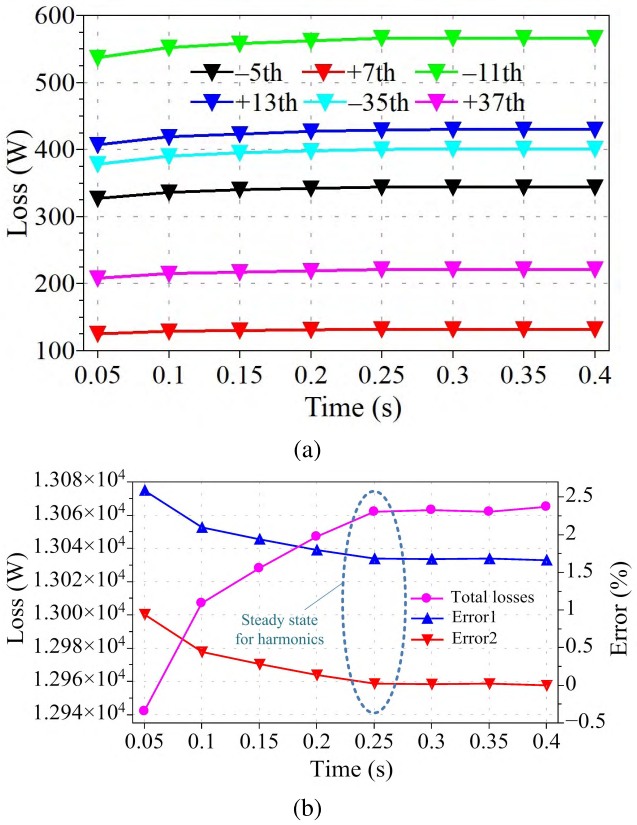

FIGURE 13. (a) Main harmonic rotor eddy-eddy current losses estimated by the improved VPMHM model during the transient. (b) Total rotor eddy-current losses estimated by the improved VPMHM model during the transient.

at 0.40 s. In Fig. 13(b), Error 1 and Error 2 denote the errors with respect to the total losses (13286 W) from the normal FEM model and the total losses (13065 W) in the steady state from the improved VPMHM model. This figure also reveals that the harmonic transients are completed at around 0.25 s, which can help to reduce the simulation time from 280 h to 190 h (40 h in total for the normal FEM model and the fundamental VPMHM model, and 150 h for the harmonic VPMHM models). However, if small errors can be accepted, the simulation time can be reduced to 70 h (40 h in total for the normal FEM model and the fundamental VPMHM model, and 30 h for the harmonic VPMHM models) with Error 1 of 2.59% and Error 2 of 0.94%. The machine studied here is a high-speed IM with a 200 Hz supply frequency, and therefore, the calculation takes time. For a similar 50 Hz machine, the simulation would be much faster (about 18 h in total).

The results and discussion above confirm that the improved VPMHM model is capable of determining the transients for harmonics, and thus, it can be used to significantly accelerate the simulation time with an acceptably small error.

V. CONCLUSION

The solid-rotor eddy-current losses can be mitigated efficiently, after the harmonic losses are correctly analyzed. To accurately separate the solid-rotor eddy-current harmonic losses for a high-speed IM from the total rotor losses, an improved VPHMH model and a computational algorithm were presented in this paper. The 2-D fast Fourier transform was used to distinguish the time-spatial harmonic components in the air-gap flux density. Two different improved VPMHM models were described to calculate the rotor eddy-current losses. The results of the two models proved to be close to each other, and they both provided about 98.5% of the total losses obtained from the normal FEM model. With the improved VPMHM model, it was also possible to obtain the distributions of the rotor eddy current and penetration depth caused by a particular harmonic. Moreover, the simulation time was further optimized for the

VPMHM model, based on the fact the high-order harmonics had shorter transients than the fundamental. Finally, the total simulation time was reduced by 30% (fully completing the harmonic transients) and 75% (with some acceptable errors). With the simulation results, it is possible to mitigate the rotor losses correspondingly. For example, according to the harmonic losses in Fig. 9, it reveals that it is more worthy to suppress the −11th and +13th harmonic losses instead of the stator slot harmonic losses. Therefore, the rotor skewed can be utilized and optimized towards the −11th and +13th harmonics. The VPMHM model also has the potential to be further developed to estimate other electromagnetic characteristics (e.g. harmonic torques) in electrical machines in the future.

ACKNOWLEDGMENT

The authors would like to thank Dr. Hanna Niemelä, Lappeenranta University of Technology, for her linguistic assistance in the preparation of this manuscript.

REFERENCES

[1] A. Smirnov, N. Uzhegov, T. Sillanpää, J. Pyrhönen, and O. Pyrhönen, "High-speed electrical machine with active magnetic bearing system optimization," *IEEE Trans. Ind. Electron.*, vol. 64, no. 12, pp. 9876–9885, Dec. 2017.

[2] Y. Zhang, S. McLoone, and W. Cao, "Electromagnetic loss modeling and demagnetization analysis for high speed permanent magnet machine," *IEEE Trans. Magn.*, vol. 54, no. 3, Mar. 2018, Art. no. 8200405.

[3] C. Gong and T. Habetler, "A novel rotor design for ultra-high speed switched reluctance machines over 1 million rpm," in *Proc. IEEE Int. Electric Mach. Drives Conf. (IEMDC)*, May 2017, pp. 1–6.

[4] D. H. Lee, T. H. Pham, and J. W. Ahn, "Design and operation characteristics of four-two pole high-speed SRM for torque ripple reduction," *IEEE Trans. Ind. Electron.*, vol. 60, no. 9, pp. 3637–3643, Sep. 2013.

[5] D. Gerada, A. Mebarki, N. L. Brown, C. Gerada, A. Cavagnino, and A. Boglietti, "High-speed electrical machines: Technologies, trends, and developments," *IEEE Trans. Ind. Electron.*, vol. 61, no. 6, pp. 2946–2959, Jun. 2014.

[6] J. Pyrhonen, J. Nerg, P. Kurronen, and U. Lauber, "High-speed, 8 mw, solid-rotor induction motor for gas compression," in *Proc. 18th Int. Conf. Electr. Machines*, Sep. 2008, pp. 1–6.

[7] J. B. Danilevich, V. N. Antipov, I. Y. Kruchinina, and Y. P. Khozikov, "Design considerations of submersible unprotected solid-rotor induction motor," in *Proc. 18th Int. Conf. Electr. Mach.*, Sep. 2008, pp. 1–4.

[8] N. Uzhegov, J. Barta, J. Kurfürst, C. Ondrusek, and J. Pyrhönen, "Comparison of high-speed electrical motors for a turbo circulator application," *IEEE Trans. Ind. Appl.*, vol. 53, no. 5, pp. 4308–4317, Sep. 2017.

[9] J. Pyrhonen, J. Nerg, P. Kurronen, and U. Lauber, "High-speed high-output solid-rotor induction-motor technology for gas compression," *IEEE Trans. Ind. Electron.*, vol. 57, no. 1, pp. 272–280, Jan. 2010.

[10] P. Lazari, J. Wang, and B. Sen, "3-D effects of rotor step-skews in permanent magnet-assisted synchronous reluctance machines," *IEEE Trans. Magn.*, vol. 51, no. 11, pp. 1–4, Nov. 2015.

[11] J. Wang, S. L. Ho, W. N. Fu, and Y. H. Wang, "Design and analysis of a novel traveling wave induction heating system with magnetic slot wedges for heating moving thin strips," *IEEE Trans. Magn.*, vol. 46, no. 6, pp. 2175–2178, Jun. 2010.

[12] O. Misir, S. M. Raziee, N. Hammouche, C. Klaus, R. Kluge, and B. Ponick, "Prediction of losses and efficiency for three-phase induction machines equipped with combined star-delta windings," *IEEE Trans. Ind. Appl.*, vol. 53, no. 4, pp. 3579–3587, Jul./Aug. 2017.

[13] M. Markovic and Y. Perriard, "Analytical solution for rotor eddy-current losses in a slotless permanent-magnet motor: The case of current sheet excitation," *IEEE Trans. Magn.*, vol. 44, no. 3, pp. 386–393, Mar. 2008.

[14] M. Markovic and Y. Perriard, "An analytical determination of eddy-current losses in a configuration with a rotating permanent magnet," *IEEE Trans. Magn.*, vol. 43, no. 8, pp. 3380–3386, Aug. 2007.

[15] Z. Q. Zhu, K. Ng, N. Schofield, and D. Howe, "Improved analytical modelling of rotor eddy current loss in brushless machines equipped with surface-mounted permanent magnets," *IEE Proc. Electr. Power Appl.*, vol. 151, no. 6, pp. 641–650, Nov. 2004.

[16] Y. Zhang, K. Lu, and Y. Ye, "Permanent magnet eddy current loss analysis of a novel motor integrated permanent magnet gear," *IEEE Trans. Magn.*, vol. 48, no. 11, pp. 3005–3008, Nov. 2012.

[17] M. Koo, J. Choi, J. Jeong, J. Kim, and Y. Park, "Comparative analysis of eddy current loss in permanent magnet synchronous generator considering PM shape and skew effect for wind power generation," in *Proc. IEEE Int. Magn. Conf. (INTERMAG)*, May 2015, p. 1.

[18] C. Di, I. Petrov, and J. J. Pyrhönen, "Modeling and mitigation of rotor eddy-current losses in high-speed solid-rotor induction machines by a virtual permanent magnet harmonic machine," *IEEE Trans. Magn.*, vol. 54, no. 12, pp. 1–12, Dec. 2018.

[19] C. Wang, X. Bao, S. Xu, Y. Zhou, W. Xu, and Y. Chen, "Analysis of vibration and noise for different skewed slot-type squirrel-cage induction motors," *IEEE Trans. Magn.*, vol. 53, no. 11, Nov. 2017, Art. no. 8206006.

[20] I. Petrov, M. Niemelä, P. Ponomarev, and J. Pyrhönen, "Rotor surface ferrite permanent magnets in electrical machines: Advantages and limitations," *IEEE Trans. Ind. Electron.*, vol. 64, no. 7, pp. 5314–5322, Jul. 2017.

[21] J. Pyrhonen, T. Jokinen, and V. Hrabovcova, *Design Rotating Electronic Machines*. Hoboken, NJ, USA: Wiley, 2013.

[22] G. T. Paula, J. R. B. A. Monteiro, T. E. P. Almeida, M. P. Santana, W. C. A. Pereira, and M. L. Aguiar, "Investigation of reluctance torque in a BLDC motor using frozen permeability method and equivalent air-gap analysis," *IEEE Latin Amer. Trans.*, vol. 14, no. 8, pp. 3678–3686, Aug. 2016.

[23] G. Li, Z. Q. Zhu, and G. Jewell, "Performance investigation of hybrid excited switched flux permanent magnet machines using frozen permeability method," *IET Electr. Power Appl.*, vol. 9, no. 9, pp. 586–594, Nov. 2015.

CHONG DI was born in Wuxi, China, in 1991. He received the B.Eng. and M.Eng. degrees in electrical engineering from the Hefei University of Technology, Hefei, China, in 2014 and 2017, respectively. He is currently pursuing the D.Sc. degree with the Department of Electrical Engineering, Lappeenranta University of Technology, Finland.

His research interest includes high-speed electrical machines.

ILYA PETROV received the D.Sc. degree from the Lappeenranta University of Technology, Finland, in 2015, where he is currently a Fellow Researcher with the Department of Electrical Engineering.

JUHA J. PYRHÖNEN (M'06–SM'17) born in Kuusankoski, Finland, in 1957. He received the D.Sc. degree from the Lappeenranta University of Technology (LUT), Finland, in 1991.

He was a Professor of electrical machines and drives with LUT, in 1997. He is currently engaged with the research and development of electric motors and power-electronic-controlled drives. He is also studying possibilities of using carbon-based materials in electrical machines. He has wide experience in the research and development of special electric drives for distributed power production, and traction and high-speed applications. Permanent magnet materials and applying them in machines have an important role in his research.